AUT Journal of Electrical Engineering

AUT J. Elec. Eng., 52(1) (2020) 9-18
DOI: 10.22060/eej.2020.16603.5292

A Full-Duplex, Dual-Polarization 10Gbps Radio over Fiber system with wavelength reuse for upstream signal

Masoud Deyranlou[1,*], Alireza Maleki Javan[2]

[1] MSc, Electrical Engineering Department, South Tehran Branch, Tehran, Iran
[2] PhD, Aeronautical University of Science and technology, Tehran, Iran

ABSTRACT: This study presents a full-duplex Radio-over-Fiber (RoF) system providing the users' wireless access with a bit rate of 10 Gbps over 40 GHz radio carrier. This system can be used in a centralized radio access network (C-RAN) architecture because we provide a fully analog front haul link between central station and base station. We can consider it as infrastructure between remote radio heads (RRHs) and baseband units (BBUs). The most appropriate choices in our case are using left and right-side bands of the DSB spectrum for both uplink and downlink streams and modulation of the data signal on both polarization of the optical carrier, as well as simplifying system structure, the bit rate of the proposed system, raised significantly. Furthermore, a method was provided to create redundancy for the optical fiber path and enhance system stability in case of a fiber cut. Optical external modulation is considered to be a good possibility to generate the optical mm-wave signal with high spectral purity. The transmission performance of the signal is analyzed in detail by analytical formulations and a full-duplex RoF link is built to verify our theoretical analysis results based on the simulation. Furthermore, the impacts of the fiber chromatic dispersion have been compensated in the RoF system with the dual-polarization carrier signal.

Review History:
Received: 2019-06-19
Revised: 2020-03-09
Accepted: 2020-03-09
Available Online: 2020-06-01

Keywords:
Radio-over-Fiber (RoF)
Employing DSB spectrum
Dual polarization carrier
External modulation
Full duplex

1. INTRODUCTION

Radio-over-fiber is a new technology that integrates optical waves and radio frequency signals and uses optical fibers as a media to facilitate wireless accessibility. The integration and convergence of wired and wireless networks is a promising solution to the increasing demand for higher bandwidth. Moreover, the radio-over-fiber (RoF) technology has recently attracted significant attention as an alternative transport technology for the mobile fronthaul network (MFN) of the 5th generation (5G) wireless communication systems [16].

Optical mm-wave signal generation is a key technique to realize low cost and high transmission performance in RoF-based optical wireless access networks [2]. Many complex methods have been presented for transmission of radio signals through optical fibers such as heterodyne technique with optical phase locking, electrical sub-harmonic injection, and external modulation. Optical external modulation is considered to be a good possibility to generate the optical mm-wave signal with high spectral purity. High spectral purity is usually specified through the phase-noise referenced at carrier power at certain offset from the carrier frequency and is, therefore, the most appropriate choice in our case. Achieving an increased bandwidth and employing the smallest number of Mach-Zehnder modulators possible while maintaining the signal quality are considered among the main challenges in the above-mentioned methods. A new scheme for full-duplex transmission of data signals was presented by employing the Double Side Band spectrum. In this case, one sideband is allocated to the uplink, and the other to the downlink [3-7]. Also, we implemented dual-polarization modulation in RoF system with wavelength reuse structure to increase bandwidth four times higher than similar works [1]. Furthermore, the transmission performance of the downlink and uplink was improved significantly Although the bitrate increasing [1,19]. According to the theoretical calculations and the measured bit error rates of the simulation, the binary data modulated on both polarizations can be individually detectable.

In this paper, we propose a full-duplex RoF link with a novel method to generate a 40GHzmm wave signal from a 20GHz RF oscillator at the base station. We used a Mach Zehnder modulator to generate the DSB optical mm-wave at the central station, as shown in Fig. 2b-2, this spectrum has first-order coefficients of 20GHz RF signal. If we assume 193.1THz as central frequency, 193.12THz is the positive first-order sideband and 193.8THz is the negative first-order sideband of the DSB spectrum. Since only the positive first-order sideband is used to carry the downlink signal, in the uplink, the negative part of the optical carrier of the downlink mm-wave signal is abstracted and is reused to bear the upstream data [1]. The optically generated adjacent

*Corresponding author's email: mdeyranlou@yahoo.com

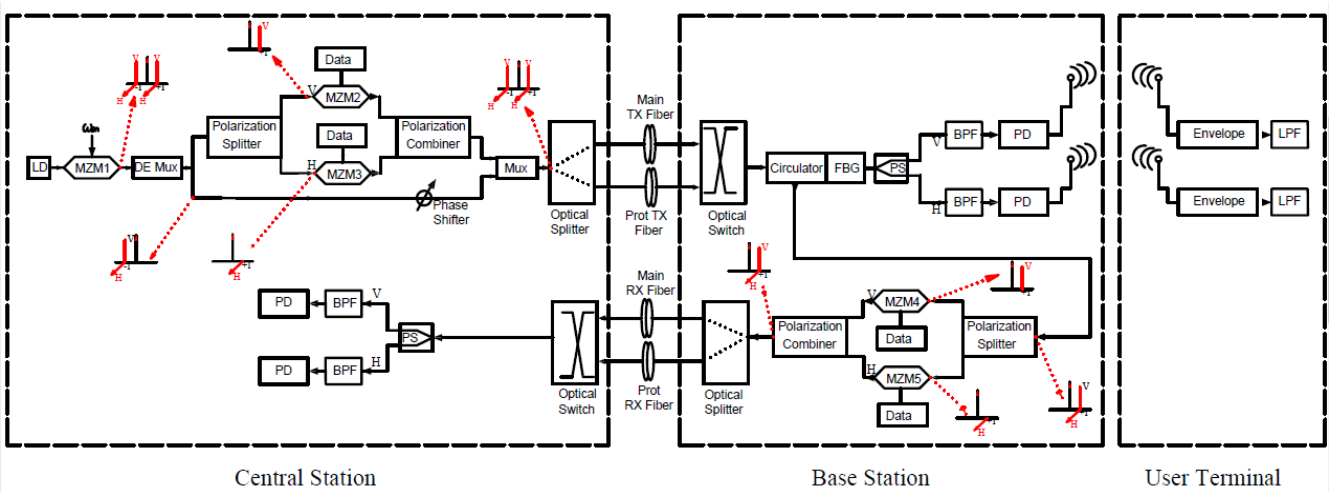

Fig. 1. Model of the full-duplex RoF system

channel interference (O-ACI) issue in the wavelength-reuse multi-channel radio-over-fiber systems is a big challenge. By tuning the bias voltage of the main modulator of the dual parallel Mach–Zehnder modulator, the amplitude, and phase of the optical carrier are controlled to improve the O-ACI [17]. Modulation of the data signal on both polarizations of sidebands increased the bit rate of the system to double. The transmission performance of the signal is analyzed in details by analytical formulations in theorical modeling section and a full duplex RoF link is built to verify our theoretical analysis results based on the simulation [8-11].

This paper is organized as follows: In Section 2, the theoretical modeling of the RoF link is described in detail. In Section 3, a dual polarization, full-duplex RoF link is built to verify our theoretical analysis results based on the simulation. section 4, presents the results and discussion. Finally, a conclusion is given in Section 5.

2. THEORETICAL OR EXPERIMENTAL MODELING

The principle diagram of the proposed full-duplex RoF system based on wireless access and wavelength reuse is shown in Fig. 1.

In Fig.1, LD represents the laser diode, RF is the radio signal source, MZM is the Mach-Zehnder modulator, CIRC is the optical circulator, FBG is the fiber Bragg grating, DATA is the source of data signal, PD is the photodiode, BPF is the Band-pass filter, and LPF is the low-pass filter.

A narrow linewidth light wave is generated using a continuous wave (CW) laser diode LD is expressed by Eq. 1. The continuous-wave laser is used as an optical source. When the azimuth angle of the CW laser source is 45 degrees, it can generate two linear polarities on the horizontal and vertical axes. The continuous-wave laser is used as an optical source and split into X-Y polarized signals using polarization splitter. This wave, as illustrated by Fig. 1, has vertical and horizontal polarities demonstrated by x and y.

$$E_0(t) = E_{0(X)} exp(j\omega_c t) + E_{0(y)} exp(j\omega_c t) \quad (1)$$

In Eq. 1, $E_0(x)$, $E_0(y)$ also ωc describe the amplitudes of the horizontal and vertical components and the phase of the electrical field, respectively. The light wave is injected into the first Mach-Zehnder modulator. The modulator is biased at the maximum transmission point to enhance the first-order sidebands and suppress the remaining. An RF local oscillator with phase ω_m, voltage amplitude V_{RF}=2V, and frequency shift of 180° between the two arms is applied to the Mach-Zehnder modulator. The output light of the modulator is obtained from Eq. 2. The second kind of Bessel function was used to derive Eq. 2. As evident, the output signal of the modulator has first-order positive and negative sidebands with horizontal and vertical components. The resulting signal is the DSB spectrum, where the data signal is modulated on the first-order positive sideband for both polarities.

$$\begin{aligned} E_{out1}(t) &= \frac{E_{0(X)}e^{j\omega_c t}}{10^{\frac{inloss}{20}}}\left[\frac{1}{2}e^{j\pi(cos(\omega_m t+\pi)/V_{\pi RF})} + \frac{1}{2}e^{j\pi(cos(\omega_m t)/V_{\pi RF})}\right] \\ &+ \frac{E_{0(Y)}e^{j\omega_c t}}{10^{\frac{inloss}{20}}}\left[\frac{1}{2}e^{j\pi(cos(\omega_m t+\pi)/V_{\pi RF})} + \frac{1}{2}e^{j\pi(cos(\omega_m t)/V_{\pi RF})}\right] \\ &= \frac{1}{2}\frac{E_{0(X)}e^{j\omega_c t}}{10^{\frac{inloss}{20}}}\left[\sum_{n=-\infty}^{n=+\infty}(-1)^n J_n(m) j^n e^{jn\omega_m t} + j^n e^{jn\omega_m t}\right] \\ &+ \frac{1}{2}\frac{E_{0(Y)}e^{j\omega_c t}}{10^{\frac{inloss}{20}}}\left[\sum_{n=-\infty}^{n=+\infty}(-1)^n J_n(m) j^n e^{jn\omega_m t} + j^n e^{jn\omega_m t}\right] \\ &\approx \frac{E_{0(X)}e^{j\omega_c t}}{10^{\frac{inloss}{20}}}\left[J_0(m) - J_1(m)e^{j2\omega_m t} - J_{-1}(m)e^{-j2\omega_m t}\right] \\ &+ \frac{E_{0(Y)}e^{j\omega_c t}}{10^{\frac{inloss}{20}}}\left[J_0(m) - J_1(m)e^{j2\omega_m t} - J_{-1}(m)e^{-j2\omega_m t}\right] \end{aligned} \quad (2)$$

In Eq. 2, inloss, indicates internal losses, V_π is the bias voltage of the Mach-Zehnder modulator, m is the RF modulation factor expressed as $m=\pi V_{RF}/V_\pi$ and $J_n()$ is the n-th order Bessel function of the second kind, where n assumes integer values. As mentioned earlier, the output of modulator MZM_1 contains positive and negative first-order optical carrier signals with vertical and horizontal components. After splitting, the positive first-order sideband is abstracted and intensity-modulated by the downstream unipolar binary data

signal K(t) and S(t) associated with vertical and horizontal polarities using the MZM_2 and MZM_3 modulators. After that, the horizontal and vertical polarities are again combined to form the positive first-order sideband. The output of the second modulator is:

$$E_{out_{2(t)}} = \frac{E_{in(t)}}{10^{\frac{inloss}{20}}}\left[\frac{1}{2}e^{\left(j\pi\left(V_{2(t)}/V_\pi\right)+j\pi\left(V_{b2}/V_\pi\right)\right)} + \frac{1}{2}e^{\left(j\pi\left(V_{1(t)}/V_\pi\right)+j\pi\left(V_{b1}/V_\pi\right)\right)}\right] \quad (3)$$

V1(t) and V2(t) are the amplitudes of RF signal applied to mach-Zehnder modulator. By taking into account the parameters, Eq. 3 can be rewritten as follows:

$$E_{in} = -\left[E_{0(X)}J_1(m)exp\left[j\left(\omega_c+2\omega_m\right)t\right]/10^{\frac{inloss}{20}} + E_{0(y)}J_1(m)exp\left[j\left(\omega_c+2\omega_m\right)t\right]/10^{\frac{inloss}{20}}\right] \quad (4)$$

$$V_2(t) = V_2S(t) = V_2K(t)$$

$$V_1(t) = V_1S(t) = V_2K(t)$$

$$V_{b1} = V_b$$

$$V_{b2} = V_b + V_\pi$$

$$V_2 = -V_1$$

As shown in Eq. 4, E_{in} includes both horizontal and vertical components assuming:

$$V_b = \frac{V_\pi}{2}, V_2 = \frac{V_\pi}{2} \quad (5)$$

Hence, the output light is obtained as follows.

$$E_{out3}(t) = \frac{E_0(X)}{10^{\frac{inloss}{10}}}e^{j\left(\omega_c+2_{\omega_m}\right)t}J_{1(m)}sin\left[\frac{\pi}{2}S(t)\right] + \frac{E_0(Y)}{10^{\frac{inloss}{10}}}e^{j\left(\omega_c+2_{\omega_m}\right)t}J_{1(m)}sin\left[\frac{\pi}{2}K(t)\right] \quad (5)$$

$$= \frac{E_0(X)}{10^{\frac{inloss}{10}}}J_1(m)e^{j\left(\omega_c+2_{\omega_m}\right)t}A(t) + \frac{E_0(X)}{10^{\frac{inloss}{10}}}J_1(m)e^{j\left(\omega_c+2_{\omega_m}\right)t}B(t)$$

In order to simplify the equations, we assume:

$$A(t) = \frac{sin\left[\frac{\pi S(t)}{2}\right]}{10^{\frac{inloss}{20}}} = B(t) = \frac{sin\left[\frac{\pi K(t)}{2}\right]}{10^{\frac{inloss}{20}}} \quad (6)$$

Since the sidebands of the DSB optical millimeter-wave signal are separated, processed and recombined, they experience a phase shift, polarization rotation, and coherence change. However, we can improve the coherence by using the short optical path or employing a narrow-linewidth laser. If the high-quality equipment for separating, processing, and recombining of the light waves are utilized, the coherence of the three light carriers can be improved extremely. An optical phase shifter provides a phase shift of Δφ for the negative sideband. Then, after adjustment of polarization, the three components are recombined to form the resulting DSB signal defined by Eq. 8. As stated by Eq. 8, the data signals are modulated on both polarities of the positive sideband.

$$E_{out_4}(t) = \frac{E_0(X)}{10^{\frac{inloss}{10}}}\left[J_0(m)e^{j\omega_c t} - J_{-1}(m)e^{j\left((\omega_c-2\omega_m)t+\Delta_\varphi\right)}J_1(m)A(t)e^{j((\omega_c-2\omega_m)t)}\right] + \frac{E_0(Y)}{10^{\frac{inloss}{10}}}\left[J_0(m)e^{j\omega_c t} - J_{-1}(m)e^{j\left((\omega_c-2\omega_m)t+\Delta_\varphi\right)}J_1(m)B(t)e^{j((\omega_c-2\omega_m)t)}\right] \quad (8)$$

Upon transmission of an optical DSB signal over fiber, the optical fiber dispersion phenomenon causes the three optical components to travel at different speeds. By denoting the propagation constant and attenuation coefficient of the fiber by β(ω) and κ, respectively, the mm-wave DSB signal, after traveling a distance of z, is obtained from Eq. 9.

$$E_{out_5}(z,t) = \frac{E_0(X)}{10^{\frac{inloss}{10}}}e^{-\frac{\kappa z}{2}}\left[J_0(m)e^{j(\omega_c t-\beta(\omega_c)z)} - J_{-1}(m)e^{j\left((\omega_c-2\omega_m)t-\beta(\omega_c-2\omega_m)z+\Delta_\varphi\right)} + J_1(m)A(t-t')e^{j((\omega_c+2\omega_m)t-\beta(\omega_c+2\omega_m)z)}\right] + \frac{E_0(Y)}{10^{\frac{inloss}{10}}}e^{-\frac{\kappa z}{2}}\left[J_0(m)e^{j(\omega_c t-\beta(\omega_c)z)} - J_{-1}(m)e^{j\left((\omega_c-2\omega_m)t-\beta(\omega_c-2\omega_m)z+\Delta_\varphi\right)} + J_1(m)A(t-t')e^{j((\omega_c+2\omega_m)t-\beta(\omega_c+2\omega_m)z)}\right] \quad (9)$$

It is assumed:

$$t' = \frac{\beta\left(\omega_c+2\omega_m\right)z}{\left(\omega_c+2\omega_m\right)} \quad (10)$$

Given the short distance between the transmitter and receiver, and considering an optical fiber length of 20 km, the polarization rotation, which causes problems in splitting the horizontal and vertical components, was neglected. Considering that the optical carrier has stronger amplitude than the sidebands, a fiber Bragg grating with the bandwidth

smaller than 2ωm and the central frequency at ω_c is used to separate the carrier of the uplink at the base station. Care must be taken in selecting the FBG bandwidth in the real system because the FBG is sensitive to the environmental conditions. If the FBG has a wide bandwidth, the drifted edges of the passband will reduce the amplitude of the two sidebands. If the FBG with the narrower bandwidth is used, the drift of the central frequency will fluctuate the power of the reflected optical carrier greatly. Hence, by representing the transmission coefficient as α, the mm-wave DSB signal after passing through the FBG is obtained as:

$$E_{out5}(z,t) = \frac{E_{0(X)}}{10^{\frac{inloss}{20}}} e^{-\frac{\kappa z}{2}} [aJ_0(m)e^{j[\omega_c t-\beta(\omega_c)z]}$$
$$-J_{-1}(m)e^{j[(\omega_c-\omega_m)t-\beta(\omega_c-\omega_m)z+\Delta_\varphi]}+$$
$$J_1(m)A(t-t')e^{j[(\omega_c-\omega_m)t-\beta(\omega_c+\omega_m)z]}]$$
$$+\frac{E_{0(Y)}}{10^{\frac{inloss}{20}}} e^{-\frac{\kappa z}{2}} [aJ_0(m)e^{j[\omega_c t-\beta(\omega_c)z]} \quad (11)$$
$$-J_{-1}(m)e^{j[(\omega_c-\omega_m)t-\beta(\omega_c-\omega_m)z+\Delta_\varphi]}$$
$$+J_1(m)B(t-t')e^{j[(\omega_c-\omega_m)t-\beta(\omega_c+\omega_m)z]}]$$

We may write the following equation for the optical carrier signal split to be used in the uplink:

$$E_c(t) = \frac{E_{0(X)}}{10^{\frac{inloss}{20}}} e^{-\frac{\hat{e}z}{2}} (1-a)J_0(m)e^{j[\omega_c t-\beta(\omega_c)z]} + \quad (12)$$
$$\frac{E_{0(Y)}}{10^{\frac{inloss}{20}}} e^{-\frac{\hat{e}z}{2}} (1-a)J_0(m)e^{j[\omega_c t-\beta(\omega_c)z]}$$

The optical signal represented in Eq. 11 is injected in a high-speed photodiode so that the ω_m component of the optical flow is:

$$I_{\omega_m}(z,t) = \frac{2\mu E_{0(X)}^2}{10^{\frac{inloss}{20}}} e^{-\kappa z} aJ_0(m)J_1(m)$$
$$[A(t-t')cos[\omega_m t+\beta(\omega_c)z-\beta(\omega_c+\omega_m)z]$$
$$-cos[\omega_m t-\beta(\omega_c)z+\beta(\omega_c-\omega_m)z-\Delta_\varphi]] \quad (13)$$
$$+\frac{2\mu E_{0(Y)}^2}{10^{\frac{inloss}{20}}} e^{-\kappa z} aJ_0(m)J_1(m)$$
$$[B(t-t')cos[\omega_m t+\beta(\omega_c)z-\beta(\omega_c+\omega_m)z]$$
$$-cos[\omega_m t-\beta(\omega_c)z+\beta(\omega_c-\omega_m)z-\Delta_\varphi]]$$

Where $J_1(m) = J_{-1}(m)$. We assume that the two parts experience different phase changes due to the different sideband speeds caused by optical dispersion in the fiber. Fortunately, a phase shifter at the negative first-order sideband can apply the changes as required by Eq. 14:

$$\omega_m t-\beta(\omega_c)z+\beta(\omega_c-\omega_m)z-\Delta_\varphi = \frac{\pi(2n+1)}{2} \quad (14)$$

We can reduce the degradation of the fading effect by shifting the fading null points. This can be done by using the phase shift Δφ on the negative sideband using the optical phase shifter.

$$I_{\omega_m}(z,t) = \frac{2\mu E_{0(X)}^2}{10^{\frac{inloss}{20}}} e^{-\kappa z} aJ_0(m)J_1(m) \quad (15)$$
$$[[A(t-t')-1]cos[\omega_m t+\beta(\omega_c)z-\beta(\omega_c+\omega_m)z]]+$$
$$\frac{2\mu E_{0(Y)}^2}{10^{\frac{inloss}{20}}} e^{-\kappa z} aJ_0(m)J_1(m)$$
$$[[B(t-t')-1]cos[\omega_m t+\beta(\omega_c)z-\beta(\omega_c+\omega_m)z]]$$

The mm-wave signal in the uplink carrying the binary signal can be demodulated to the baseband of S′ (t) through envelope detection:

$$A'(t) = S'(t)cos(\omega' t), B'(t) = K'(t)cos(\omega' t) \quad (16)$$

As expressed by Eq. 17, the data signal generated at the user terminal for the uplink, which is denoted by S′ (t) and K′ (t), is modulated on the optical carrier of the return link in the base station and transmitted over the uplink. The following relation can be written for the optical signal carrying data:

$$E_1'(t) = \frac{E_0(X)}{10^{\frac{inloss}{20}}} e^{\frac{-\kappa z}{2}} (1-a)J_0(m)e^{j[\omega_c t-\beta(\omega_c t)z]}S'(t)$$
$$+\frac{E_0(Y)}{10^{\frac{inloss}{20}}} e^{\frac{-\kappa z}{2}} (1-a)J_0(m)e^{j[\omega_c t-\beta(\omega_c t)z]}K'(t) \quad (17)$$

The baseband signal of the uplink is returned to the central station through a single-mode optical fiber with the length of z′:

$$E_2'(t) = \frac{E_0(X)}{10^{\frac{inloss}{20}}} e^{\frac{-\kappa z}{2}} (1-a)J_0(m)e^{j[\omega_c t-\beta(\omega_c t)z]}S'(t-t'')$$
$$+\frac{E_0(Y)}{10^{\frac{inloss}{20}}} e^{\frac{-\kappa z}{2}} (1-a)J_0(m)e^{j[\omega_c t-\beta(\omega_c t)z]}K'(t-t'') \quad (18)$$

Where:

$$t'' = \frac{\beta(\omega_c z')}{\omega_c} \tag{19}$$

The delay t" is due to optical dispersion caused by the uplink fiber. The uplink signal can be directly detected by a high-speed photodiode:

$$\begin{aligned} I_1'(z',t) &= \mu|E_2'(z',t)|^2 \\ &= \mu\frac{E_0^2(X)}{10^{\frac{inloss}{10}}}(1-a)^2 J_0^2(m)e^{-\kappa z}S'^2(t-t'') + \\ &\mu\frac{E_0^2(Y)}{10^{\frac{inloss}{10}}}(1-a)^2 J_0^2(m)e^{-\kappa z}K'^2(t-t'') \\ &= \mu\frac{E_0^2(X)}{10^{\frac{inloss}{10}}}(1-a)^2 J_0^2(m)e^{-\kappa z}S'(t-t'') + \\ &\mu\frac{E_0^2(Y)}{10^{\frac{inloss}{10}}}(1-a)^2 J_0^2(m)e^{-\kappa z}K'(t-t'') \end{aligned} \tag{20}$$

$$S'^2(t-t'') = S'(t-t''), K'^2(t-t'') = K'(t-t'') \tag{21}$$

Here, Eq. 21 is used for unipolar binary signals S′ (t) and K′ (t). As shown, the fading effect was compensated by using phase shifter and, hence, the downlink was protected from the distortion effects caused by the time shift of the code edges distortion. Since only one sideband carries the downlink signal, the upstream data is transmitted to the central station through another optical carrier, which, as shown, has low distortion and keeps the simplicity of the system structure. Moreover, it appropriately transmits the vertical and horizontal components which contain data signals, along the optical fiber and they can be split at the receiver. This link is well capable of transmitting data signals at a speed of 10 Gbps through a single-mode optical fiber while producing an acceptable quality. In the following section, the model proposed for simulation and the respective results are presented.

3. SIMULATION AND NUMERICAL RESULTS:

Fig. 2a illustrates the detailed block diagram of our system. Calculations and simulations have been done using optisystem software. The simulation was conducted in this section, and the behavior of signal waveform for uplink and downlink obtained from the simulation results were presented. The diagram shows central and base stations separately for easy understanding.

In Fig. 2a, LD, laser diode; MZM, Mach-Zehnder modulator; PCO, polarization controller; WDM, wavelength division multiplexer; PS, polarization splitter; PC, polarization combiner; OC, optical coupler; PD, photodiode; BPF, Band-pass filter; LPF, low-pass filter; EYE, eye diagram;

Fig. 2b illustrates the optical signal spectrums in different parts. The locations of each of these spectrums are specified by 1-6 in Fig. 2a. The output of a continuous-wave (CW) laser diode working at λ = 1550 nm (Fig.2b.1) with a line width of 100 MHz injected into the dual-drive Mach-Zehnder modulator (MZM_1). Also, the first and second bias voltages applied to this modulator were -2.8 v and 0.5 v, respectively. Furthermore, an RF oscillator with a frequency of 20 GHz and amplitude of 2v was applied to the electrical input of the MZM_1. The phase of the RF signal was set at 90°. The same RF oscillator was used for the next electrical input of the modulator, with the phase shift of 180°. By applying the appropriate parameters to the MZM_1 modulator, the spectrum of the DSB optical millimeter-wave signal with the frequency spacing of 20GHz can be generated. Fig. 2b.2 shows the DSB spectrum generated by the MZM_1. After abstracting

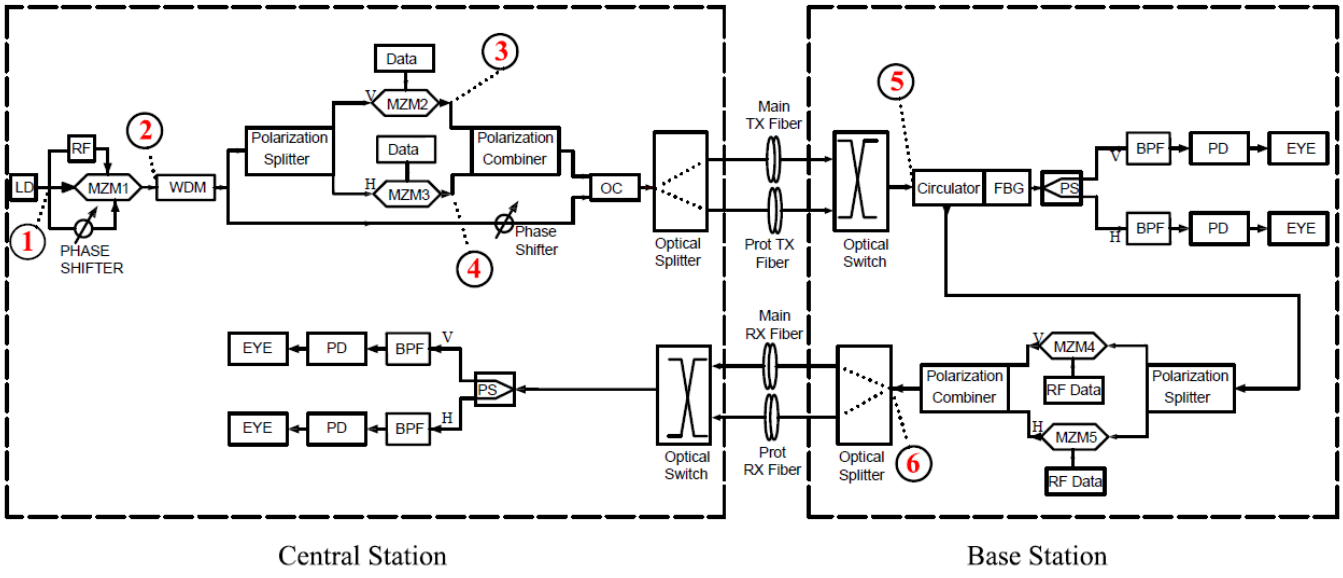

Fig. 2a. Block diagram of the RoF system for full-duplex transmission at a speed of 10 Gbps.

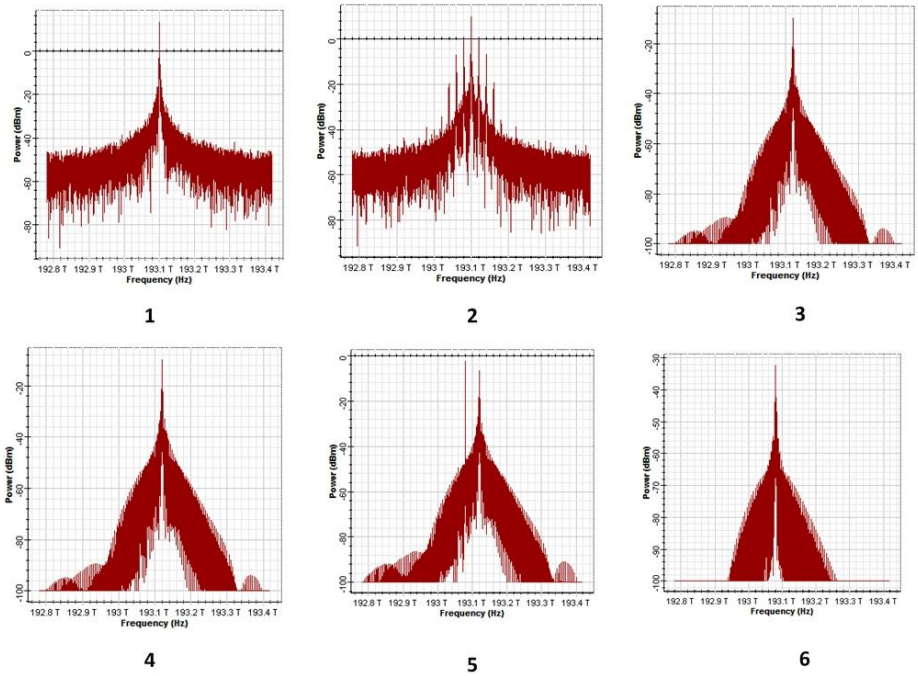

Fig. 2b. The optical signal spectrums of figure 2a

the positive first-order sideband of the DSB spectrum using WDM, the vertical and horizontal polarization of the positive first-order sideband split to vertical and horizontal components. The 5Gbps binary data signals are modulated using MZM_2 and MZM_3 modulators on vertical and horizontal components. Figs. 2b.3 and 4 show the spectrums made by the MZM_2 and MZM_3 respectively. The modulation index of modulators is as follows:

$MZM_1 = 1.66\ \pi$, $MZM_2 = \pi/2$ and $MZM_3 = \pi/2$.

Furthermore, an optical phase shifter with phase shift of 165° is placed in the path of the negative first-order sideband. By changing the phase shift and Length of the fiber and simultaneous monitoring of BER and Q-factor, the best amount of shift for fiber with a length of up to 20 km was obtained. As mentioned in above section, Eq. (15) shows that the signal code A(t) and B(t) carried by the RF at ωm has only a constant time delay of t′ and so is free from the distortion caused by fiber chromatic dispersion. Therefore, the phase shift obtained along with the values considered for optical signal strength and other parameters are considered to be the best Q-Factor. After a polarization aligning, the two sidebands are combined to generate the DSB optical mm-wave signals by the optical coupler. The generated DSB spectrum contains two main sidebands, one of the sidebands is modulated using the binary signal and the other is shifted by an optical phase shifter. Then the DSB signal enters to splitter. A splitter that has a slight power loss transmits the input signal on both output ports. these ports are connected to two optical fibers which used for each uplink and downlink. In the case of one fiber cut, the signal is alive in the other fiber because an optical switch with a switching time of ns was used in destination to switch over the connected fiber to prevent signal interruption. This method was provided to create redundancy for the optical fiber path and enhance system stability in case of a fiber cut. Single-mode fibers were used with a dispersion of 16.75 ps/nm km and power attenuation coefficient of 0.2 dB/km, which is similar in characteristics to typical fibers. The length of the optical fiber was considered 10 km in the simulation but it can increase up to 20km in this system. The optical switch measures the strength of the input optical signal of both fibers and selects the stronger one. In case of an interruption in each, the second fiber is automatically replaced. An FBG with a central frequency of ωc and bandwidth smaller than 2ωm is used at the base station to split a part of the optical carrier. The fiber Bragg grating reflection and transmission parameters must be carefully selected. The center of the Fiber Bragg Grating reflection spectrum is 193.08THz. This FBG is used to abstract part of the center optical carrier to bear the uplink signal. The transmission spectrum of FBG is 193.12THz. A polarization splitter is then used to split the horizontal and vertical components, after that, a high-speed photodiode of PIN type converts the optical signal, to an electric signal. An electrical signal with a frequency of 40 GHz is obtained for both polarizations by using a band-pass filter of Bessel type. According to ITU-R recommendation, 36.0-40.5 GHz is allocated to the fixed and mobile services, because the propagation characteristics of this bands are ideally suited to short-range digital and analog radio systems; also 24 to 40 GHz is expected to be Global 5G Bands. To investigate the signal quality of downlink, a low-pass filter is applied to the data signal to be analyzed using an eye diagram analyzer. On the other side, for uplink, the optical carrier signal split by Bragg grating enters a polarization splitter, after which the

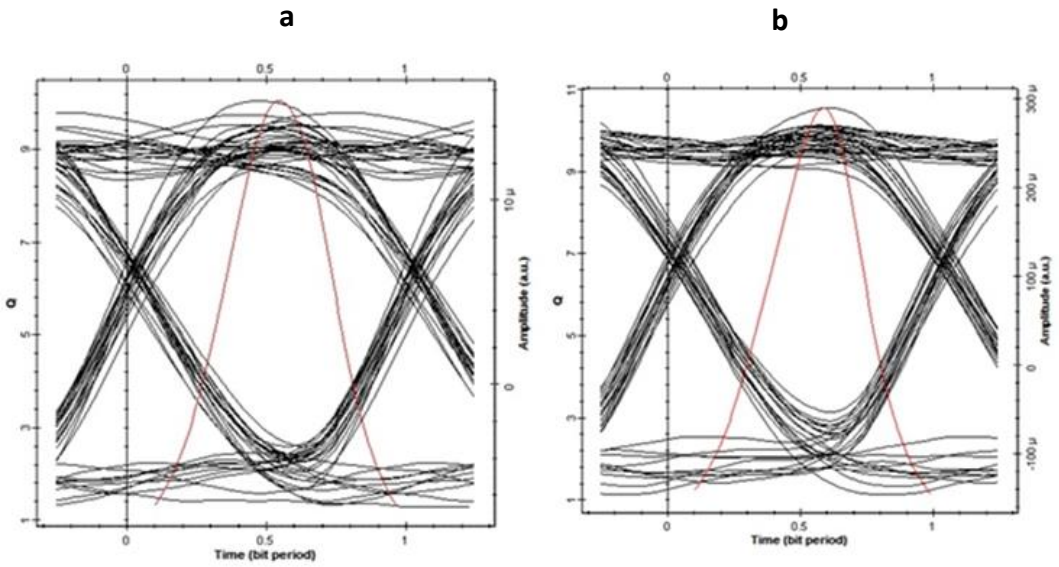

Fig.3. a. The eye and Q-factor diagrams for the vertical component of the downlink. b. The eye and Q-factor diagrams for the horizontal component of the downlink.

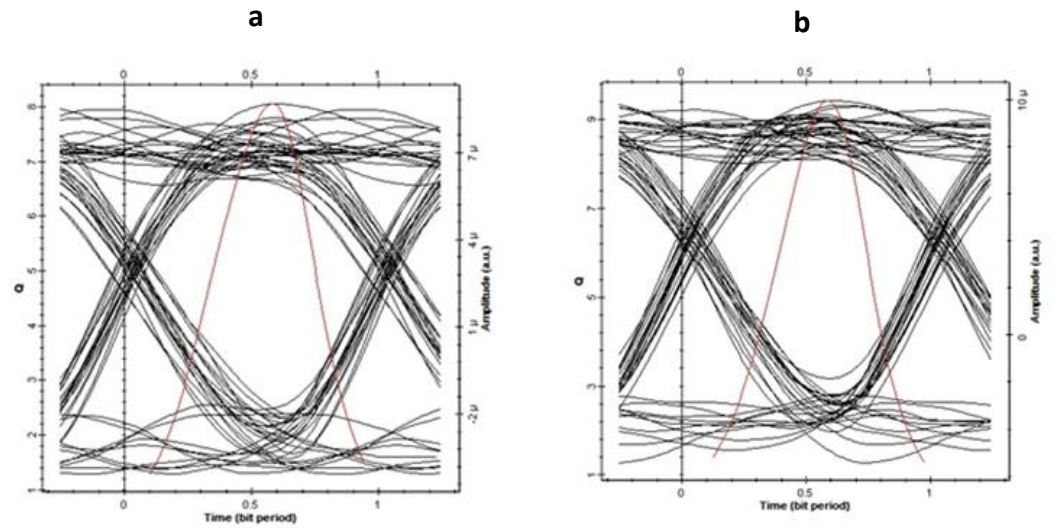

Fig.4. a. The eye and Q-factor diagrams for the vertical component of the uplink. b. The eye and Q-factor diagrams for the horizontal component of the uplink.

data signal of the uplink is modulated on the vertical and horizontal components using MZM4 and MZM5. Then, a polarization combiner is used to combine the horizontal and vertical components to be transmitted over the fiber. Fig.2b.6 shows the output spectrum of this coupler. Moreover, the first and second bias voltages of these modulators were 1.8 v and -4 v, respectively, and the modulation voltage was set to 2.5 v. In the receiver station, a high-speed photodiode was used to convert the received optical signal to an electrical one. Afterward, low-pass filters were applied to abstract the data signal to be analyzed using the eye diagram analyzer.

4. THE RESULTS AND DISCUSSION:

It can be seen that the system can present good access in the 40GHz wireless band which is also confirmed by the eye patterns in Figs. 3-4. This is because there is no fading effect for the 40GHz mm-wave signal. As predicted by our above theoretical modeling the fading effect was bypassed by using phase shifter and both polarizations of the downlink and uplink were protected from the distortion effects caused by the time shift of the code edges distortion. Furthermore, the data signals also immune to the time shift of the code edges according to the eye diagrams in Figs. 3-4. According to the theoretical calculations and the measured bit error rates from the simulation, the binary data modulated on both polarizations can be individually detectable. Also, by limiting the optical fiber length and controlling the polarization of the carrier signals in the central station and base station the

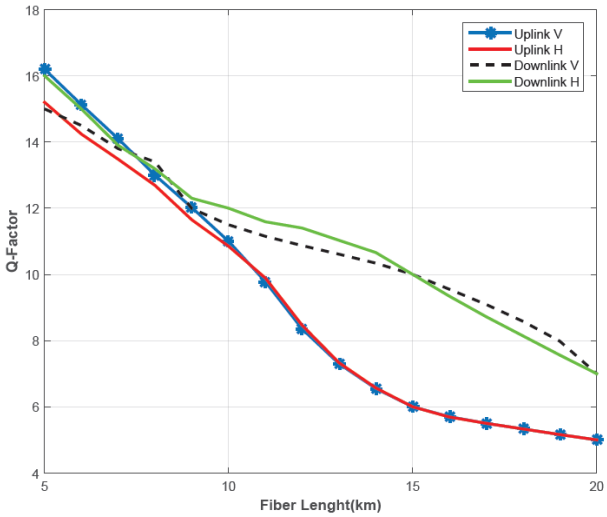

Fig. 5. Diagram of Q-factor with respect to the length of optical fiber for the uplink and downlink.

polarization cross-talk effect is compensated.

The eye diagram of the horizontal and vertical components for the downlink is presented in Fig. 3a and 3b, respectively. Furthermore, Fig. 4a and 4b show the eye diagrams for the same components for the uplink, individually. ITU has stated that the minimum rate of BER for Radio over Fiber systems must be below than 10^{-9}. The value of the Q-factor depends on the value of BER because the value of the Q-factor increases when the BER decreases. There are only two possible signal levels in binary digital communication systems and each of these signal levels may have a different average noise associated with it. This means that there are essentially two discrete signal-to-noise ratios, which are associated with the two possible signal levels. To calculate the overall probability of bit error, both the signal to noise ratio must be considered. The combination of two discrete SNRs into a single quantity providing a convenient measure of overall system quality is called the Q factor. If we compare the sampled voltage v(t) to a reference value γ called the decision threshold. If the v(t) is greater than the γ, binary one has to be transmitted and if it is less than γ then binary zero has to transmit. The major error caused in making the right decision is due to the noise added to the received data assuming perfect synchronization between bitstream and the bit clock. Indeed, The Q factor is the difference of the mean values of the two signal levels (level for a "1" bit and level for a "0" bit) divided by the sum of the noise standard deviations at the two signal levels. A larger number in the result means that the pulse is relatively free from noise [21].

In our system, for the Q-factor of 7, the BER is about 10^{-9}. Thus, our system should have a value of Q-factor higher than 7 to perform a very good Performance. The signal power, BER, and Q-factor of downlink in the base station for 10km fiber are -12dBm, 10^{-13}, and 12, sequentially. The eye diagrams obtained from the simulation are presented in Fig. 4a and 4b. As evident, the diagrams are wide and have acceptable noise and distortion peak, as well as low timing error. The Q-factor diagram concerning the length of the optical fiber is shown in Fig. 5, which was achieved by increasing the length of the fiber and measuring the Q-factor. From the simulated results which are taken with the eye diagram analyzer, it is clear that as the length of the optical fiber varies, parameters of the optical fiber that are mainly Q-factor and BER also change. Physical parameters such as noise, chromatic dispersion, losses, and polarization or non-linear property can affect the signal and ultimately cause a bit error in the radio over fiber communication. Additionally, high values of the Q-factor are due to the high Optical signal to noise ratio, which means the BER is reduced. In this paper, the length of the optical fiber varies in the km ranges from 5 km to 20 km and simulation output gives the maximum Q-factor of 16 for length L=5km. The signal power, BER, and Q-factor of the uplink are -18dBm, 10^{-11}, and 11, respectively. The eye diagrams obtained from the simulation are presented in Figs. 4a and 4b. Moreover, the diagram displayed in Fig. 5 shows the values of this parameter by increasing the length of the fiber up to 20 km.

5. THE CONCLUSION

The investigation results of the full-duplex RoF system suggest that the quality of the data-carrying signal on a single-mode, 10 km optical fiber was maintained by considering a redundancy link to prevent connection interruptions when the primary fiber is down. In summary, a DSB carrier signal is initially generated that uses the right and left sidebands, respectively, for the downlink and uplink. Then, horizontal and vertical polarities of the right sideband are split, with a 5 Gbps data signal modulated on each. Both polarities are then combined and transmitted on single-mode optical fiber, resulting in a transmission speed of 10 Gbps for the system. The reverse is applied for the uplink. Due to the short fiber optic length used in this system and the effects of vertically and horizontally polarization, it is possible to ignore the polarization cross-talk effects. The purpose of

the use of orthogonal polarizations simultaneously with the DSB spectrum and the implication of this strategy is to bring about future developments and not merely an increase in capacity. With some configuration in this system, the data transmission capacity can increase significantly. Hence, based on the conducted analysis, it can be concluded that the eye diagram obtained from the simulation was fully wide and had an appropriate noise and distortion peak, as well as a low timing error. The signal-to-noise ratio and receiver sensitivity were also analyzed. Based on the analysis, the system stability was improved compared to the other similar studies, in addition to achieving an increase in bitrate. As shown in Fig 5, the Q-factor for the horizontal and vertical components of the up and downlink signals is at its highest value. In the case of the present study, we used one sideband of DSB for uplink and the other for the downlink signal. The path of the optical carrier signal for the downlink is 10km and the path for uplinks optical carrier signal is 20km. so the difference between eye diagrams of uplink and downlink is because of different fiber loss. Single-mode fiber supports two different polarization states. Fast and slow axes have different group velocities. Therefore, the small difference between V and H polarizations in eye diagrams is because of Different Group Delay and Polarization Dispersion of optical fiber. It should be noted that this difference in our system is very low due to the short fiber optic length. By adjusting the appropriate phase shift and applying some configurations, the best Q-factor can be obtained for fiber lengths up to 20 km. As you can see in Fig. 5, the behaviors of the Q-Factor for the horizontal and vertical polarization of the downlink link are similar to each other. This situation is also similar to uplink.

REFERENCES

[1] G. Cheng, B. Guo, S. Liu, W. Fang, A novel full-duplex radio-over-fiber system based on dual octupling-frequency for 82GHz W-band radio frequency and wavelength reuse for uplink connection, Optik, 125(15) (2014) 4072-4076.

[2] Y. Chen, A. Wen, L. Shang, Y. Wang, A full-duplex radio-over-fiber link with 12-tupling mm-wave generation and wavelength reuse for upstream signal, Optics & Laser Technology, 43(7) (2011) 1167-1171.

[3] L. Combi, A. Matera, A. Gatto, P. Parolari, P. Boffi, U. Spagnolini, Radio-over-modes for C-RAN architecture with smart optical resources assignment, in: 2017 IEEE International Conference on Communications (ICC), 2017, pp. 1-6.

[4] Z. Jia, J. Yu, G. Ellinas, G.-K. Chang, Key Enabling Technologies for Optical–Wireless Networks: Optical Millimeter-Wave Generation, Wavelength Reuse, and Architecture, Journal of Lightwave Technology, 25(11) (2007) 3452-3471.

[5] L.A. Johansson, A.J. Seeds, Millimeter-wave modulated optical signal generation with high spectral purity and wide-locking bandwidth using a fiber-integrated optical injection phase-lock loop, IEEE Photonics Technology Letters, 12(6) (2000) 690-692.

[6] B.G. Kim, S.H. Bae, H. Kim, Y.C. Chung, RoF-Based Mobile Fronthaul Networks Implemented by Using DML and EML for 5G Wireless Communication Systems, Journal of Lightwave Technology, 36(14) (2018) 2874-2881.

[7] L. Kumar, V. Sharma, A. Singh, Feasibility and modelling for convergence of optical-wireless network – A review, AEU - International Journal of Electronics and Communications, 80 (2017) 144-156.

[8] M. Lv, A. Yang, Y. Hua, S. Shen, J. Cui, Y.-n. Sun, Simultaneous modulation and transmission of 10-Gb/s baseband and 60-GHz microwave signals in a radio-over-fiber system, Optics Communications, 283(21) (2010) 4203-4207.

[9] J. Ma, L. Chen, X. Xin, J. Yu, C. Yu, Z. Dong, Q. Zhang, Transmission of a 40 GHz optical millimeter wave generated by quadrupling a 10 GHz local oscillator via a Mach–Zehnder modulator, Journal of Optics A: Pure and Applied Optics, 11(6) (2009) 065406.

[10] J. Ma, Y. Li, A full-duplex multiband access radio-over-fiber link with frequency multiplying millimeter-wave generation and wavelength reuse for upstream signal, Optics Communications, 334 (2015) 22-26.

[11] J. Ma, J. Yu, C. Yu, X. Xin, X. Sang, Q. Zhang, 64GHz optical millimeter-wave generation by octupling 8GHz local oscillator via a nested LiNbO3 modulator, Optics & Laser Technology, 42(2) (2010) 264-268.

[12] J. Ma, J. Yu, C. Yu, X. Xin, J. Zeng, L. Chen, Fiber Dispersion Influence on Transmission of the Optical Millimeter-Waves Generated Using LN-MZM Intensity Modulation, Journal of Lightwave Technology, 25(11) (2007) 3244-3256.

[13] M. Ogusu, K. Inagaki, Y. Mizuguchi, T. Ohira, Multiplexing of millimeter-wave signals for fiber-radio links by direct modulation of a two-mode locked Fabry-Pe/spl acute/rot laser, IEEE Transactions on Microwave Theory and Techniques, 52(2) (2004) 498-507.

[14] R. Puerta, J. Yu, X. Li, Y. Xu, J.J.V. Olmos, I.T. Monroy, Single-Carrier Dual-Polarization 328-Gb/s Wireless Transmission in a D-Band Millimeter Wave 2 × 2 MU-MIMO Radio-Over-Fiber System, Journal of Lightwave Technology, 36(2) (2018) 587-593.

[15] Y. Qin, J. Sun, Frequency sextupling technique using two cascaded dual-electrode Mach–Zehnder modulators interleaved with Gaussian optical band-pass filter, Optics Communications, 285(12) (2012) 2911-2916.

[16] L. Sainawi, K. Ismail, Receiver Performance Improvement in Radio over Fiber Network Transmission, in, 2017.

[17] L. Shang, A. Wen, B. Li, T. Wang, Y. Chen, M.a. Li, A filterless optical millimeter-wave generation based on frequency octupling, Optik, 123(13) (2012) 1183-1186.

[18] Z. Tang, S. Pan, A Full-Duplex Radio-Over-Fiber Link Based on a Dual-Polarization Mach–Zehnder Modulator, IEEE Photonics Technology Letters, 28(8) (2016) 852-855.

[19] F. Wei, S. Li, X. Zheng, H. Zhang, B. Zhou, Improvement of Optically Generated Adjacent Channel Interference in RoF Systems, IEEE Photonics Technology Letters, 25(12) (2013) 1137-1140.

[20] R. Zhu, M. Hui, D. Shen, X. Zhang, Mach-Zehnder modulator modulated radio-over-fiber transmission system using dual wavelength linearization, Optics Communications, 385 (2017) 229-237.

[21] P. Kaur, D. Purohit, G. Singh, A Study on CS-RZ-ASK Modulation Format for Long Haul Optical Communication, IJIREEICE, 3 (2015) 51-54.

HOW TO CITE THIS ARTICLE

M. Deyranlou, A.R. Maleki Javan, A Full-Duplex, Dual-Polarization 10Gbps Radio over Fiber system with wavelength reuse for upstream signal, AUT J. Elec. Eng., 52(1) (2020) 9-18.

DOI: 10.22060/eej.2020.16603.5292